Journal of Analytical Science and Technology

RESEARCH ARTICLE Open Access

ZnO-TiO_2 doped polyacrylonitrile nano fiber-Mat for elimination of Cr (VI) from polluted water

Şerife Parlayıcı[1*], Adem Yar[2], Erol Pehlivan[1] and Ahmet Avcı[3]

Abstract

PAN nanofiber-Mat (n-fib@Mat), PAN/ZnO n-fib@Mat, and PAN/ZnO-TiO_2 n-fib@Mat were prepared via electrospinning method. Their high adsorption capacities against dissolved Cr (VI) ions make them as super adsorbents for water treatment. The structure of n-fib@Mat was investigated using XRD, FTIR, SEM, and TEM techniques. The effects of selected parameters such as contact time, initial concentration, and n-fib@Mat amount were assessed in a fixed bed reactor. It was found that the adsorption capacities of PAN n-fib@Mat, PAN/ZnO n-fib@Mat, and PAN/ZnO-TiO_2 n-fib@Mat were pH-dependent and the optimal pH value was between 2.1 and 2.2. The adsorption was rapid, and the equilibrium was reached within 240 min to remove of Cr (VI) ions for PAN/ZnO-TiO_2 n-fib@Mat and 360 min for PAN n-fib@Mat and PAN-ZnO n-fib@Mat. Langmuir isotherms model is preferred for PAN n-fib@Mat, PAN-ZnO n-fib@Mat, and PAN/ZnO-TiO_2 n-fib@Mat for Cr (VI) adsorption. The equilibrium adsorption capacities are 153.85 mg/g, 234.52 mg/g, and 333.43 mg/g for PAN n-fib@Mat, PAN/ZnO n-fib@Mat, and PAN/ZnO-TiO_2 n-fib@Mat for Cr (VI), respectively. The produced n-fib@Mat showed excellent removal ability for Cr (VI). The adsorption kinetic was obeyed pseudo-second-order reaction rate.

Keywords: Electrospun, Chromium, Adsorption, Nanofiber-Mat, Equilibrium

Introduction

Heavy metals in polluted waters become common problems in developing countries. They are widely used in different industries and have high soluble in polluted water (Matos et al. 2017). Toxic metals must be removed from wastewater in a short time. There are many heavy metal ions in wastewater such as Cr, Cd, Pb, Ni, As, and Co. Hexavalent chromium (Cr (VI)) is a very poisonous substance (Qiu et al. 2014; Parlayici 2019). For this reason, the elimination of Cr (VI) from natural waters and sewage plants is one of the great targets to get rid of from the toxicity. Cr (VI) is one of the poisonous substances and is originated from electroplating, mining industry, metal plating, leather tanning, photography, steel manufacturing, dye, and textiles industries (Qiu et al. 2014; Cao et al. 2014; Beheshti et al. 2016; Lv et al. 2019; Liu et al. 2018; Wang et al. 2013; Yuan et al. 2010).

Large amounts of chromium in the supply of waste are harmful to human health and environment (Parlayici and Pehlivan 2019). Many methods such as solvent extraction, filtration (Hanif and Shahzad 2014; Solomon et al. 2013; Yang et al. 2010), ion exchange, membrane process, precipitation, and adsorption were applied to Cr (VI) elimination from contaminated wastewater (Fan et al. 2012; Kaya et al. 2014).

A new type of adsorbents is nanostructured materials that offer a greater number of Cr (VI) adsorption sites due to their high surface area. A different application that has been studied in this research is the use of *n*-fib@Mat with intrinsic or synthetic functional groups to interact or reduct of Cr (VI). *n*-fib@Mats are polymeric materials with unique mechanical, physical, and chemical properties with small size and very high surface area which can provide critical advantages for environmental applications. *n*-fib@Mats obtained by electrospinning have been of particular interest in the literature due to their ability to bridge double nano-macro structures and scales. Such a property, combined with the characteristic

* Correspondence: serife842@hotmail.com
[1]Department of Chemical Engineering, Konya Technical University, Campus, 42079 Konya, Turkey
Full list of author information is available at the end of the article

high porosity, light weight, flexibility and a low cost of *n*-fib@Mat, constitutes functionalized systems that will appear as alternative adsorbents to trap or reduce Cr (VI) from wastewater. Electrospinning, which is an electro-rheological process in recent years, is a very sensitive technique as a simple and low-cost methodology to produce mats composed of micro- or nano-fibers (Alcaraz-Espinoza et al. 2015). Currently, nano metal oxide, including nanoparticles such as ferric oxides, manganese oxides, aluminum oxides, titanium oxides, magnesium oxide,s and zinc oxides doped fibers, have been used to remove toxic metal ions (Lee and Yang 2012; Li et al. 2012; Qiu et al. 2012; Su et al. 2009).

Polyacrylonitrile (PAN) is an important polymer for the production of high-performance carbon fibers. More attention is paid to the novel kinds of thermal and solvent stable fibers. Some nanoparticles, such as ZnO and TiO_2, as a doped material, have been incorporated into the mat matrix to reduce the swelling of the polymer in solvents. Nanoparticle-doped PAN mats opened up a broad spectrum for modern research techniques. They are synthesized by forming two or more compounds with similar properties and some metal oxides such as ZnO and TiO_2 are introduced into the matrix of PAN. Today, PAN/ZnO-TiO_2 *n*-fib@Mat relates to a nanoscale between 1 and 100 nm having physical and chemical properties differ from larger particles.

In this study, we developed PAN *n*-fib@Mat, PAN/ZnO *n*-fib@Mat, and PAN/ZnO-TiO_2 *n*-fib@Mat nanofibers using electrospinning method to treat Cr (VI) pollutants. PAN/ZnO-TiO_2 *n*-fib@Mat is one of the preferred methods and the development of new *n*-fib@Mat with a high adsorption capacity and stability in various medium is highly desirable for the environmental aspect. PAN/ZnO-TiO_2 *n*-fib@Mat is an excellent adsorbent due to the advantages of high stability, efficiency, low energy consumption costs, and is the ideal choice for *many industrial applications.* They can be applied for environmental protection from toxic metals. The electrospinning method was used to prepare *n*-fib@Mat in diameters ranging from tens of nanometers to submicrometers. PAN/ZnO-TiO_2 *n*-fib@Mat can be prepared by the electrospinning process and has a higher specific active surface area and a *higher porosity* and *fine pores.* Therefore, the electrospun PAN/ZnO-TiO_2 *n*-fib@Mat was successfully used to remove Cr (VI).

In the present research, PAN/ZnO-TiO_2 *n*-fib@Mat was obtained by the electrospinning process and adsorption of Cr (VI) ion from the polluted samples was examined. The effects of contact time, pH, and initial Cr (VI) ion concentration were optimized for the adsorption processes. The batch type reactors were used for the adsorption and the equilibrium and kinetic parameters related to *n*-fib@Mats and Cr (VI) elimination with the PAN/ZnO-TiO_2 *n*-fib@Mat was evaluated. Due to superior properties, ZnO, TiO_2 of *n*-fib@Mats will be an alternative novel nano-adsorbent for removal of Cr (VI) in wastewater plants.

Experimental

Materials

All chemicals used in the experiments were of analytical grade and ultra-pure water was used for the preparation of the required solutions. The Cr (VI) stock solution was prepared by dissolving $K_2Cr_2O_7$ salt (Merck) in ultra-pure water. NaOH and HCl solutions were purchased from Merck. Standards related to the different concentrations of Cr (VI) were prepared by diluting the appropriate quantity of the Cr (VI) stock solution. PAN (MW: 150000) was obtained from Sigma-Aldrich and dimethylformamide (DMF) was obtained from Merck. ZnO and TiO_2 nanoparticles were synthesized by the arc-discharge method in Nano Material Science laboratory in Konya Technical University.

Synthesis of ZnO and TiO_2 nanoparticles

ZnO-TiO_2 nanoparticles were produced by a similar procedure by the arc discharge technique reported previously (Avcı et al. 2013; Eskizeybek et al. 2011). The arc discharge was generated between the Ti-Zn bimetal electrode acting as an anode and the Ti electrode acting as a cathode in 5 L isolated Pyrex beaker. The beaker was filled with 4 L ultra-pure water, and the arc discharge devices were completely immersed in the ultra-pure water. A high purity titanium rod with 10 mm diameter and 20 mm length was used as the cathode. Another titanium rod of 12 mm diameter and 70 mm length was drilled and replaced in the 5 mm diameter hole. The high purity uniform-shaped Zn rod with 5 mm diameter was placed into the titanium rod. This bi-metal composite rod behaved like an anode electrode during the arc-discharge. The arc-discharge was initiated in the ultra-pure water by touching the electrodes. One millimeter gap between the electrodes was controlled by a voltage regulator measuring discharge voltage in the range of 20 and 30 V to obtain a stable arc. The arc-discharge was maintained until 30 mm length of the anode electrode which was consumed during the experiment. The anode electrode was consumed by discharging until the remaining of 30 mm length of the bi-metal composite rod. The solution was kept for 3 days at room temperature to provide settling of the nanoparticles in ultra-pure water. The products were collected on silicon wafers and then dried at 80 °C under vacuum.

Figure 1 displays the typical TEM image of ZnO-TiO_2 nanoparticles where the nano-rods are ZnO and the nano-spheres are TiO_2. TEM image shows that ZnO and TiO_2 nanostructures are homogeneous distribution in the matrix and the ZnO/TiO_2 nanoparticles contain two

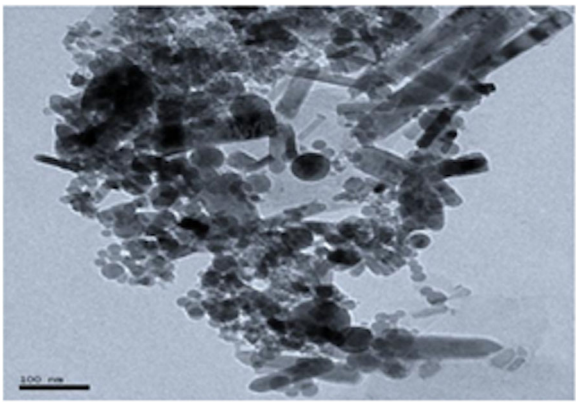

Fig. 1 Typical TEM image of ZnO + TiO_2 nanoparticles where the nano-rods are ZnO and the nano-spheres are TiO_2

different nanostructure morphologies such as nano-rods and nano-spheres. Nano-rods indicate ZnO nanostructure which has different diameters and lengths whereas the nano-spheres are TiO_2 nanoparticles with different diameters changing from 10 to 100 nm. The detailed analysis of the ZnO-TiO_2 nanoparticles was given in reference (Avcı et al. 2013).

Production of nanofibers

First, the combination of PAN and nanoparticle has been optimized to achieve good and uniform nanofibers. An ultrasonic probe was used to produce nanofibers. Then, 0.5 g of ZnO and TiO_2 nanoparticles were introduced in 10 ml DMF and then placed in an ultrasonic bath for 60 min. Thus, ZnO and TiO_2 nanoparticles were homogeneously dispersed in the mixture. Futher, 1.0 g PAN was added to the dispersed mixture of ZnO-TiO_2 nanoparticles at 60 °C for 2 h to make a viscous solution for electrospinning. The solution was then cooled to room temperature before electrospinning process. When the electrostatic repulsion force overcomes the force of surface tension of the polymer solution, the fluids spill out of the spinneret and forms an extremely fine continuous filament. Then, the prepared solution was loaded into a 10 ml syringe with 19 gauge metal needle tip. The distance between the needle tip and the square collectors was set as 15 cm. Then, the steel fabric mesh cleaned with acetone and ethanol was situated on the square collector in order to be used for the adsorption of Cr (VI). The speed of the solution was maintained by a syringe pump at a feed rate of 0.35 ml/h. An electric field passage between the needle tip and the square plate was achieved with a high-voltage power supply with a voltage of 30 kV. PAN *n*-fib@Mat, PAN/ZnO *n*-fib@Mat, and PAN/ZnO-TiO_2 *n*-fib@Mat gathered on the steel mesh on the square plate. The electrospinning process was conducted in an enclosed pet class cabin. The fabricated PAN *n*-fib@Mat, PAN/ZnO *n*-fib@Mat, and PAN/ZnO-TiO_2 *n*-fib@Mat were kept at room temperature to adsorb Cr(V) ions in the aqueous solution. The electrospinning and adsorption process were depicted in a detailed way in Fig. 2.

Applied methods

Removal methods are usually applied to the adsorption of Cr (VI) to the surface of nanoparticles embedded into the PAN *n*-fib@Mat and work effectively for estimating of the capacity. Their removal capacity depends on their porous structure and interface functionality. PAN/ZnO-TiO_2 *n*-fib@Mats are new fibers to be applied for taking away Cr (VI) in polluted water. *A series of standard* Cr (VI) solutions by appropriate *dilution* of the stock *solution were prepared for the removal experiments.* For successful Cr (VI) ion removal, a certain amount of PAN/ZnO-TiO_2 *n*-fib@Mat was contacted with 50 ml of Cr (VI) solution at a constant speed using an orbital shaker at 25 °C. After filtration, the concentration of Cr (VI) in the filtrate was defined by a UV-Vis spectrophotometer (Shimadzu UV-1700) (λ: 540 nm) using a diphenyl carbazide reagent. The entire removal of Cr (VI) was determined by taking the difference of initial concentration and total Cr (VI) concentration in the filtrate medium. Removing tests were carried out in a Pyrex beaker in laboratory conditions (25 °C).

Results and discussion

Characterization of PAN *n*-fib@Mat, PAN/ZnO *n*-fib@Mat, and PAN/ZnO-TiO_2 *n*-fib@Mat

The structural morphologies of electrospun *n*-fib@Mats are illustrated in Fig. 3. It shows that the manufactured pristine PAN *n*-fib@Mat is oriented with the diameters ranging from 50 to 350 nm with a homogeneous and a smooth surface (Fig. 3a). The structure morphologies of PAN *n*-fib@Mat were tested after they were used to adsorb Cr (VI) in the aqueous solution (Fig. 3b). During the adsorption process, PAN *n*-fib@Mat was found to be stable and tough. Any critical deterioration and cracks were not observed on the surface of the PAN *n*-fib@Mat as shown in Fig. 3b. The fiber surfaces became slightly rough, and the Cr (VI) ion residually began to appear on the surfaces of the PAN *n*-fib@Mat after subjected to the polluted with Cr (VI) solution.

It is observed that the morphological units of pristine PAN *n*-fib@Mat change with the addition of ZnO nanostructures, although the electrospinning process is performed under the same spinning parameters and conditions (Fig. 3c). In addition, the loading of ZnO nanoparticle into the PAN matrix leads to decrease nanofiber diameters to around 100 nm and affects the homogeneity of the nanofiber structure forming conical bead-like structure to the nanofiber axis compared to

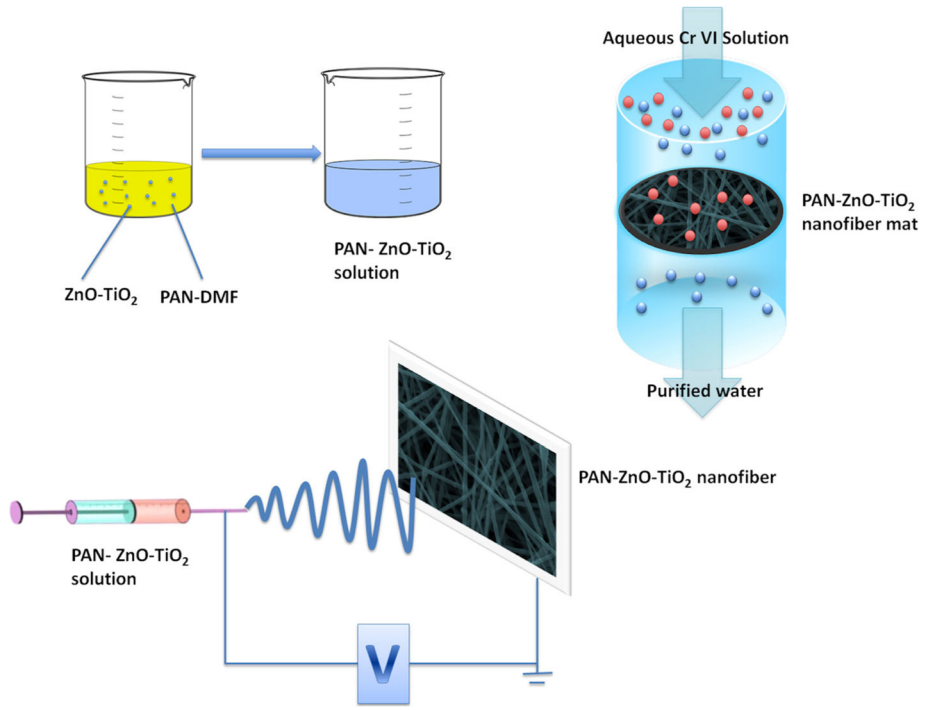

Fig. 2 The schematic of the fabrication of PAN *n*-fib@Mat decorated nanoparticle and the application for Cr (VI) removal

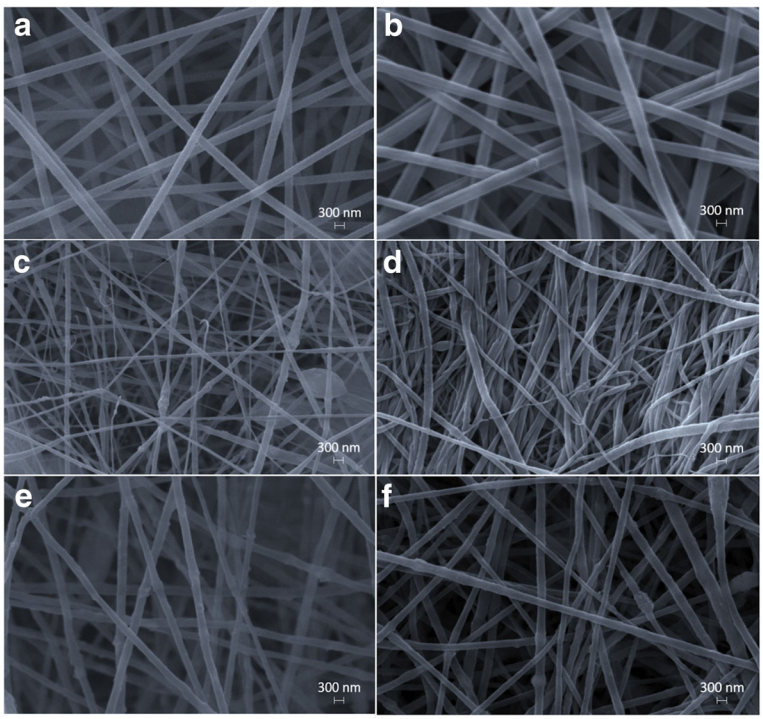

Fig. 3 SEM images **a** of PAN *n*-fib@Mat, **b** PAN *n*-fib@Mat after Cr (VI) adsorption, **c** PAN-ZnO *n*-fib@Mat, **d** PAN-ZnO *n*-fib@Mat after Cr (VI) adsorption, **e** PAN-ZnO-TiO_2 *n*-fib@Mat, and **f** PAN-ZnO-TiO_2 *n*-fib@Mat after Cr (VI) adsorption

neat PAN *n*-fib@Mat. Such morphological structures are due to the ZnO agglomerations stemming from an insufficient ZnO nanostructure dispersion in the PAN solution. The fiber diameter of PAN/ZnO *n*-fib@Mat was significantly increased following adsorption of Cr (VI) ion compared to the dry PAN/ZnO *n*-fib@Mat (Fig. 3d).

Moreover, the agglomeration of nano-ZnO caused structural inequality with the fabricated electrospun mat composite by influencing the electric field during the process. It can be seen that similar morphology was obtained with the addition of ZnO-TiO_2 for electrospun PAN/ ZnO-TiO_2 *n*-fib@Mat (Fig. 3e). However, the formation of agglomerated balls in PAN/ZnO-TiO_2 *n*-fib@Mat is smaller than of the PAN/ZnO *n*-fib@Mat. The investigation of ZnO-TiO_2-loaded *n*-fib@Mat showed that each nanofiber surface in the electrospun PAN/ ZnO-TiO_2 *n*-fib@Mat had a rough and porous structure with respect to the pristine PAN *n*-fib@Mat. The porosity structure was derived from a phase separation between the PAN/ZnO-TiO_2 *n*-fib@Mat and solvent (DMF) by evaporating the solvent in it. This structural feature morphology is probably due to the specific surface area and the porosity of PAN/ZnO *n*-fib@Mat. Further, the adsorption phenomena took place by means of diffusion of Cr (VI) ions on an inner surface of electrospun mats, and the adsorption of Cr (VI) ions performed on the outer surface of the *n*-fib@Mat. The porosity structure that may play an important role in the adsorption capacity of PAN/ZnO-TiO_2 *n*-fib@Mat was increased by introducing ZnO-TiO_2. The surface morphology of PAN/ZnO-TiO_2 *n*-fib@Mat changed without deformation after the adsorption (Fig. 3f), thus showing a coarse *n*-fib@Mat structure.

The TEM image illustrated in Fig. 4a indicates PAN *n*-fib@Mat. The average PAN *n*-fib @ Mat diameter corresponding to the SEM results is to be around 300 nm. Embedding of a hybrid nanoparticle is clearly visible in electrospun PAN *n*-fib@Mat. The dense region decorated with nanoparticle can be observed in PAN *n*-fib@Mat. On the basis of the TEM analysis, we observed that the distribution of ZnO-TiO_2 and ZnO nanoparticle in PAN *n*-fib@Mat can influence the structural features of

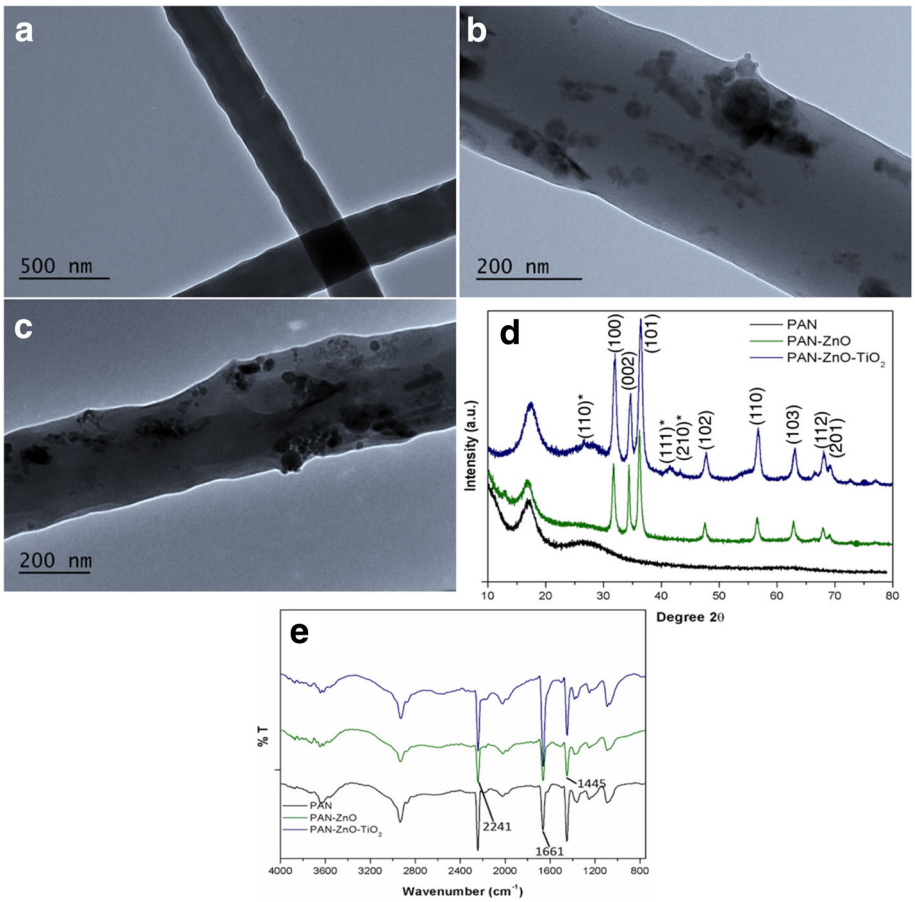

Fig. 4 Representing TEM images of **a** PAN *n*-fib@Mat, **b** PAN-ZnO *n*-fib@Mat, **c** PAN-ZnO-TiO_2 *n*-fib@Mat, and **d** XRD pattern of ZnO and TiO_2-ZnO nanoparticles immersed in *n*-fib@Mat. **e** FT-IR spectra of PAN *n*-fib@Mat, PAN-ZnO *n*-fib**b**Mat, and PAN-ZnO-TiO_2 *n*-fib@Mat

n-fib@Mat. This proves that ZnO nanoparticles were grafted through PAN *n*-fib@Mat (Fig. 4b). While the ZnO-TiO_2 nanoparticles were inserted along the PAN *n*-fib@Mat axis, some of them were attached to the surface of PAN *n*-fib@Mat as can be seen in Fig. 4c.

The XRD peaks of PAN *n*-fib@Mat, PAN/ZnO *n*-fib@-Mat, and PAN/ZnO-TiO_2 *n*-fib@Mat are shown in Fig. 4d. The pattern of pristine PAN *n*-fib@Mat shows a peak in the range 15–20° range, consistent with an index for PAN and a small peak can existed in the range of 20–30°. As obviously depicted, the PAN *n*-fib@Mat has an amorphous structure without any nanostructures. With the incorporation of ZnO nanostructures into PAN *n*-fib@Mat, the XRD patterns became stronger with respect to the pristine PAN *n*-fib@Mat. The XRD pattern of PAN/ZnO mat demonstrates peaks of hexagonal structure of ZnO with characteristic peaks [2θ = 31.76° (100), 34.42° (002), 36.25° (101), 47.53° (102), 62.85° (103), 67.97° (112), 69.08° (201)] (JPDS No. 30–1451) as well as the PAN *n*-fib@Mat. The XRD pattern and diffraction angle confirm that the ZnO nanoparticles were not only tightly deposited on PAN *n*-fib@Mat surfaces but were also embedded within the PAN *n*-fib@Mat. After introducing ZnO-TiO_2, hybrid nanostructures peaks were observed with the PAN *n*-fib@Mat peak (Esfe et al. 2017; Toghraie et al. 2016). In the case of fabricated PAN/TiO_2 mat, four characteristic peaks (2θ = 27,7°, 36,1°, 41,4°, and 54,5°) are observed. The XRD result indicates that TiO_2 nanoparticles are in the rutile phase (JCPDS no. 88–1175). However, the peaks of rutile TiO_2 that overlapped the peaks of the wurtzite ZnO are not clearly appeared because of the sharp and intense peaks of the typical wurtzite ZnO. However, the XRD pattern of pristine PAN *n*-fib@Mat became sharp in the range of 15–20°. This is because of the presence of ZnO-TiO_2 nanomaterial in the *n*-fib@Mat.

FT-IR analysis of the PAN *n*-fib@Mat, PAN/ZnO *n*-fib@-Mat, and PAN/ZnO-TiO_2 *n*-fib@Mat were given in Fig. 4e. The FT-IR spectra of PAN *n*-fib@Mat sample showed that the peaks related to C≡N bonds and CH_2 could be seen easily in the spectra. FT-IR spectra of PAN *n*-fib@Mat have many peaks that showed the existence of CH_2, C≡N, and C–H bonds. The absorption peaks that were within 2925–2935 cm^{-1} were related to C–H bonds in CH, CH_2, and CH_3 but in this range, the second low peak was observed which was related to C-H bonds (Mittal et al. 1994). Another peak was observed in the range of 2245–2248 cm^{-1} which was related to the engagement of nitrile (C≡N) bonds and specifies the nitrile group could be found in the PAN chain. The stretching vibration of the CH group leads to the characteristic peaks at 1445 cm^{-1}, 1360 cm^{-1}, 1248 cm^{-1}, and 1221 cm^{-1} (Li et al. 2014).

Effect of pH, initial Cr (VI) ion concentration, and contact time

The surface area related to the thickness of *n*-fib@Mats can affect Cr (VI) ions adsorption. Cr (VI) solutions have been treated separately with the each of *n*-fib@Mat which have a different surface area. The Cr (VI) adsorption capacity of PAN/ZnO *n*-fib@Mat and PAN/ZnO-TiO_2 *n*-fib@Mat increased when the *n*-fib@Mat's mass increased. The adsorption capacity of them reached a plateau value as seen in Fig. 5. The adsorption cannot be affected by a certain amount of *n*-fib@Mat. In addition,

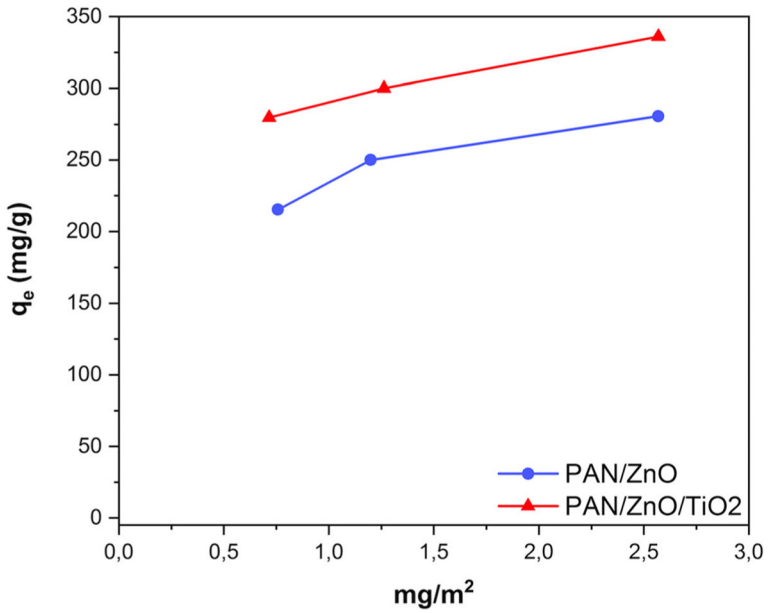

Fig. 5 Effect of *n*-fib@Mat surface area on the adsorption of Cr (VI)

the transfer of the solution through *n*-fib@Mat became more difficult after a certain thickness dimension of the *n*-fib@Mat. The optimum mass for PAN/ZnO *n*-fib@Mat and PAN/ZnO-TiO_2 *n*-fib@Mat was measured as 2.5 mg/m^2.

Figure 6 displays Cr (VI) adsorption depending on pH variation on the PAN *n*-fib@Mat, PAN ZnO *n*-fib@Mat, and PAN/ZnO-TiO_2 *n*-fib@Mat and the adsorption occurred pH values between 1.5 and 6.0. Acidity is an important factor in the adsorption of Cr (VI) in aqueous solution. It has a certain effect on the Cr (VI) solution chemistry (i.e., hydrolysis, redox reactions, polymerization, and coordination). The surface load of the adsorbents greatly affects the pH of the solution and plays an important role in the complexation of Cr (VI) ion with the adsorbent. The point of zero charges (pH_{PZC}) of PAN *n*-fib@Mat, PAN/ZnO *n*-fib@Mat, and PAN/ZnO-TiO2 *n*-fib@Mat were found in pH 7.1, 6.4, and 6.7, respectively (Fig. 7). Similar results are available in the literature (Naimi-Joubani et al. 2015; Gezici et al. 2016). Using the concept of pH_{PZC}, the surface of PAN/ZnO-TiO_2 *n*-fib@Mat will be predominant negatively charged when solution pH > 6.7, while predominant positively charged when pH < 6.7. Positively charged ions will be present on the adsorbent surface groups in acidic medium and Cr (VI) anionic form's structure can join with the complex ions in the mat. So, the adsorption of Cr (VI) is more pronounced in the pH < pH_{PZC}. The maximum adsorption was carried out around pH 2.0–2.2. The Cr (VI) adsorption mechanism is very complex due to the electrostatic interactions and the surface adsorption mechanisms. The amount of Cr (VI) transferred into *n*-fib@Mat from the solution phase decreased with increasing pH (pH > 2.4). The variation in adsorption capacity of Cr (VI) at different pH values can be attributed to the affinities of *n*-fib@Mat for the different species of Cr (VI) existing at acidic pH values namely $H_2CrO_4^o$, $HCrO_4^-$, CrO_4^{2-}, and $Cr_2O_7^{2-}$ (Pradhan et al. 2019).

ZnO-TiO_2 nanoparticles cooperated on the surface of the PAN *n*-fib@Mat can be rapidly protonated at a low pH or deprotonated at a high pH of solution phase. It is buffered with a low pH acid in the system and the functional groups of the *n*-fib@Mats were surrounded by H^+ protons. It was clear that the negatively charged Cr (VI) complex was easy to be adsorbed to the positively charged *n*-fib@Mat at low pH values due to the electronic attraction. This may happen between the surface hydroxyl groups of ZnO and TiO_2 and CrO_4^{2-} (or $Cr_2O_7^{2-}$). When the solution pH was low enough, negatively charged CrO_4^{2-} or $Cr_2O_7^{2-}$ can stick to the nanoparticle surfaces via electrostatic attraction with positively charged Zn-OH_2^+, Ti-OH_2^+, leading to the adsorption. At high pH values, there will be an electrostatic repulsion between the negatively charged CrO_4^{2-} and TiO^-, resulting in a decrease in adsorption.

The maximum Cr (VI) ion adsorption was achieved at pH 2.2 with PAN *n*-fib@Mat at 153.85 mg/g, PAN/ZnO *n*-fib@Mat at 234.52, and PAN/ZnO-TiO_2 *n*-fib@Mat was 333.43 mg/g. Adsorption increased rapidly in the equilibrium in the range of pH 1.5–2.2 and reached its peak at pH 2.2. When reaching the equilibrium, the adsorption rate slowed down. A significant increase in the

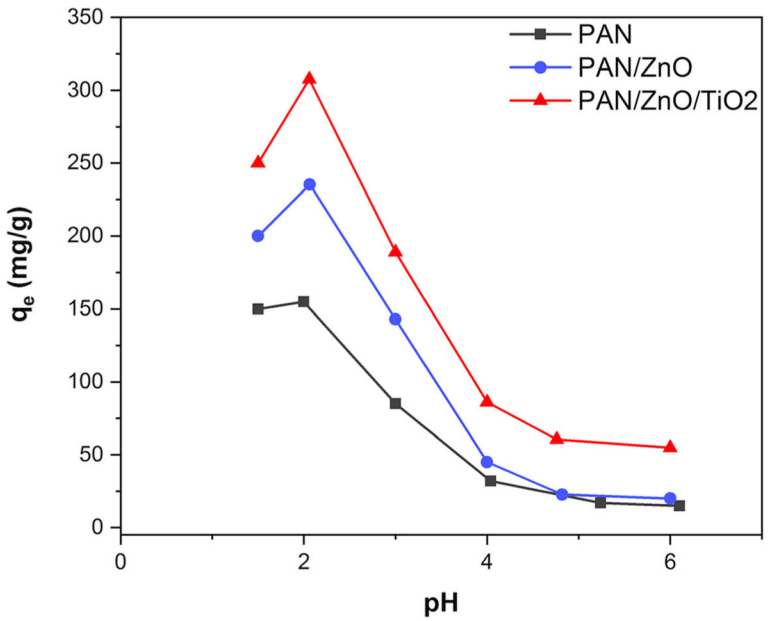

Fig. 6 The effect of pH on the adsorption of Cr (VI) using PAN based *n*-fib@Mats (pH = 1–6)

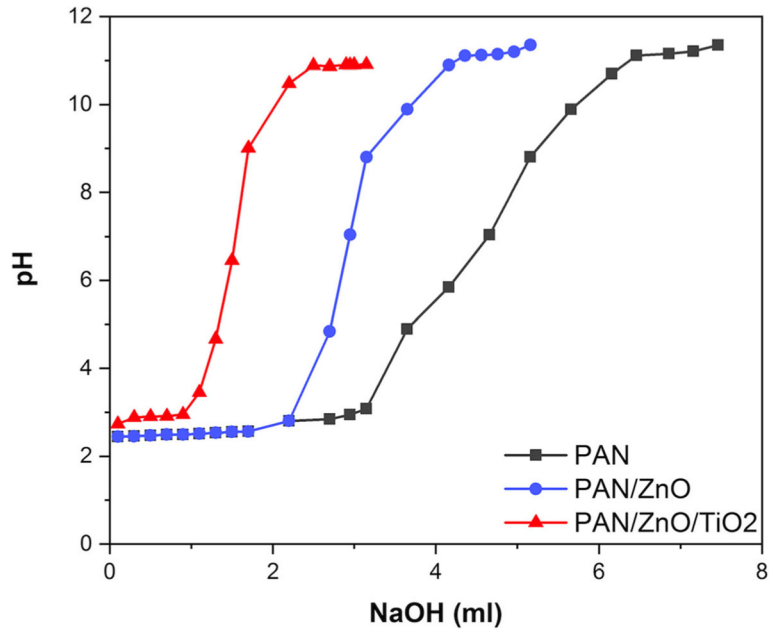

Fig. 7 pHpzc of a PAN *n*-fib@Mat, PAN/ZnO *n*-fib@Mat, and PAN/ZnO-TiO_2 *n*-fib@Mat

acidity of *n*-fib@Mat equilibrium solution was observed during the experiments.

$$\begin{array}{ccccc} & \overset{(\log = 0.38)}{} & & \overset{(\log = 6.14)}{} & \\ H_2CrO_4 & \leftrightarrow & H_2CrO_4^- & \leftrightarrow & CrO_4^{2-} \\ & & \updownarrow (\log = 1.71) & & \\ & & Cr_2O_4^{2-} & & \end{array} \quad (1)$$

When the pH of the solution is low, CrO_4^{2-} ions are transferred to $Cr_2O_7^{2-}$ with a high probability, i.e., lowering solution pH enhances the formation of $Cr_2O_7^{2-}$. It is clear that the size of $Cr_2O_7^{2-}$ion is about twice as large as a CrO_4^{2-}ion. The large size of a $Cr_2O_7^{2-}$ ion makes it difficult to penetrate through the mat and causes lower adsorption.

As the pH values of the solution phase increased, Cr (VI) was reduced to Cr (III) and the effectiveness of adsorption was decreased. The distribution of Cr (VI) species in the solution phase is shown in Eq. (1) depending on the concentration of Cr (VI) and pH of the medium. That is why the types of dichromate and chromate acid ions in solution are predominant in pH values below 3.

The adsorption of Cr (VI) in various concentrations was changed as (5, 10, 15, 20, 25, 35, 50 ppm) to determine the effect of initial adsorbate concentrations for the adsorption (Fig. 8). The adsorption of Cr (VI) was very fast due to the filling of related centers in the first step of adsorption phenomena. In the second part, the adsorption was quite slow. Freundlich and Langmuir model (Table 1) were applied for the equilibrium. These models could be expressed as follows (Parlayici and Pehlivan 2015; Langmuir 1917; Parlayici et al. 2016):

Langmuir equation (Eq. (4)):

$$q_e = \frac{A_s K_b C_e}{1 + K_b C_e} \quad (2)$$

where A_s (mmol/g) and K_b (L/mol) are the coefficients, q_e is the Cr (VI) ion amount adsorbed per unit mass of adsorbent, and C_e is the equilibrium Cr (VI) concentration in the solution phase. The empirical Freundlich isotherm based on the adsorption on heterogeneous surfaces was applied in non-linear (Eq. (3)) and logarithmic forms (Eq. (4)):

Freundlich equation:

$$\left(\frac{x}{m}\right) = kC_e^{1/n} \quad (3)$$

$$\log\left(\frac{x}{m}\right) = \log k + \frac{1}{n}\log C_e \quad (4)$$

where k and $1/n$ are the Freundlich constants indicating the relative adsorption capacity and the intensity of adsorption, respectively. X/m is the amount of Cr (VI) ions adsorbed per unit amount of adsorbent and C_e is Cr (VI) concentration at equilibrium in an aqueous phase. n values were determined as 4.48, 3.31, and 3.74 for PAN *n*-fib@Mat, PAN/ZnO *n*-fib@Mat, and PAN/ZnO-TiO_2 *n*-fib@Mat, respectively. If this value is

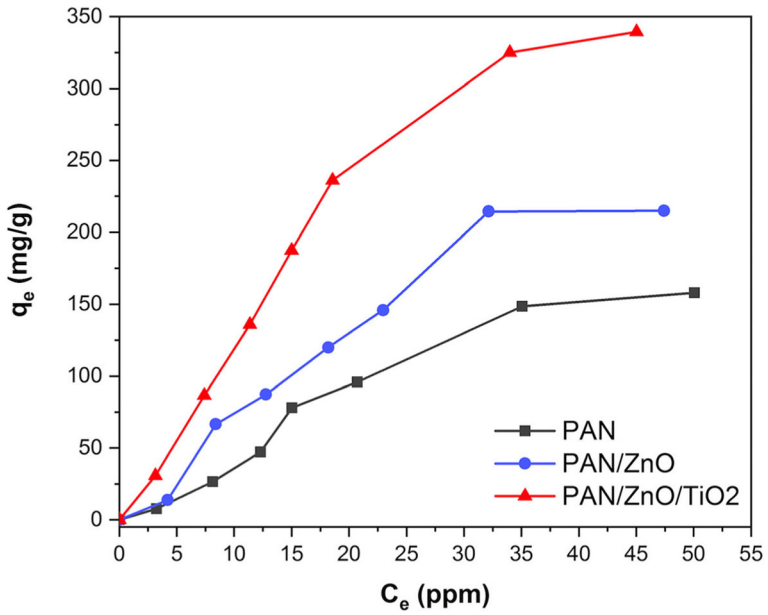

Fig. 8 Adsorption isotherm of Cr (VI) into PAN based *n*-fib@Mats as a function of initial Cr (VI) concentration

between 1 and 10, then Freundlich isotherms can be selected for adsorption.

Table 1 shows the application of adsorption equations for the adsorption isotherms. Langmuir isotherm for PAN *n*-fib@Mat, PAN/ZnO *n*-fib@Mat, and PAN/ZnO-TiO_2 *n*-fib@Mat has been found more suitable compared to the Freundlich isotherms. Table 2 shows R_L values of three types of adsorbents. R_L value tells about the adsorption either favorable or unfavorable. If the $0 < R_L < 1$ as in our case, the adsorption is favorable. Langmuir isotherm expressed the chemical adsorption and single layer adsorption. This supports the Langmuir isotherms for PAN *n*-fib@Mat, PAN/ZnO *n*-fib@Mat, and PAN/ZnO-TiO_2 *n*-fib@Mat. The maximum monolayer coverage capacity (Q) can be calculated as 153.85 mg/g for PAN *n*-fib@Mat, 234.52 mg/g for PAN/ZnO *n*-fib@Mat, and 333.43 mg/g PAN/ZnO-TiO_2 *n*-fib@Mat.

The amount of Cr (VI) retained in the *n*-fib@Mat which has a certain thickness from the aqueous solutions was investigated for a specific Cr (VI) concentration at a certain time. Figure 9 illustrates the time evaluation adsorption of Cr (VI) by PAN *n*-fib@Mat, PAN/ZnO *n*-fib@Mat, and PAN/ZnO-TiO_2 *n*-fib@Mat. The adsorption of Cr (VI) from the solution phase was completed for 5 to 1500 min at 25 °C. The adsorption trials with this *n*-fib@Mat for a certain time period showed that the adsorption increased first and then reached a constant plateau value. This may be the absence of the remaining available active places in the adsorbent matrix and the decrease in the driving force magnitude between the composite and adsorbate. As it can be seen in Fig. 9, the retention of Cr (VI) ions to the *n*-fib@Mats was very fast, because the attraction forces between Cr (VI) and *n*-fib@Mats were so strong to capture Cr (VI) ions. Adsorption time depends on the structure and features of the *n*-fib@Mat. The Cr (VI) adsorption as a function of time was slightly changed with respect to the types of the *n*-fib@Mat produced and it was between 220 and 240 mg/g for PAN/ZnO *n*-fib@Mat and 300–330 mg/g PAN/ZnO-TiO_2 *n*-fib@Mat, respectively. The equilibrium of Cr (VI) saturation was reached in 240 min for PAN/ZnO-TiO_2 *n*-fib@Mat and 360 min for PAN *n*-fib@Mat and PAN-ZnO *n*-fib@Mat. The saturation equilibrium speed of Cr (VI) depends on *n*-fib@Mat's structures. The various stages of adsorption rates of Cr (VI) observed on the surface of *n*-fib@Mat showed that the rate was rapid in the first stage and then slowed down later (Hameed et al. 2008).

Table 1 Adsorption isotherm parameters for removal of Cr (VI) by nanoparticle decorated PAN based *n*-fib@Mats

	Langmuir			Freundlich		
	Q	b	R^2	K_f	n	R^2
PAN	153.85	0.54	0.994	69.54	4.48	0.976
PAN-ZnO	234.52	0.32	0.982	82.06	3.31	0.975
PAN-ZnO-TiO_2	333.43	0.97	0.984	136.01	3.74	0.970

Table 2 R_L values of nanoparticle decorated PAN based *n*-fib@Mats

	R_L
PAN	0.0356
PAN-ZnO	0.0588
PAN-ZnO-TiO_2	0.0264

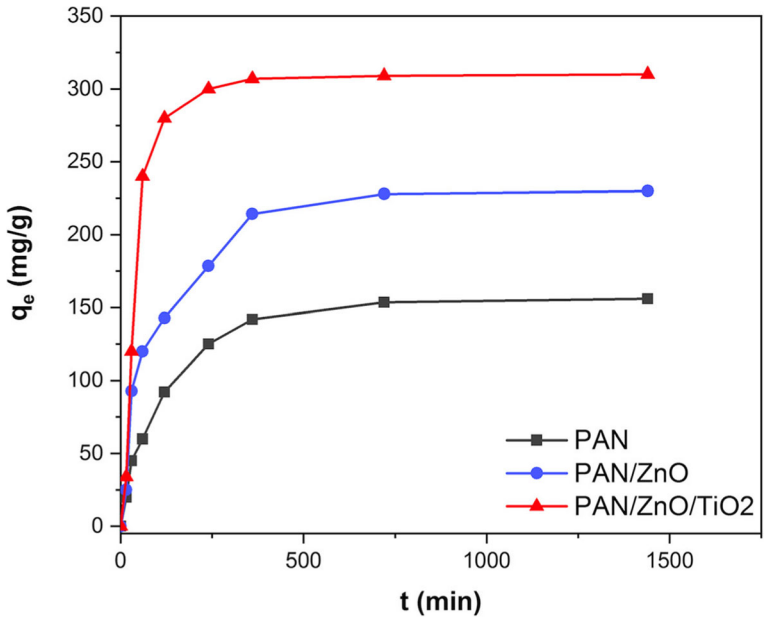

Fig. 9 Effect of contact time on the adsorption of Cr (VI) by PAN based *n*-fib@Mats

The adsorption kinetics was determined using the pseudo-first-order and pseudo-second-order kinetic models. The pseudo-second-order kinetic model was preferred and used based on the following differential equation (Koyuncu and Kul 2019). Where k_2 is the rate constant of pseudo-second-order adsorption (g mg^{-1} min^{-1}). All the rate constants were calculated and given in Table 3. The boundary condition $q_t = 0$ at $t = 0$ and the equation can be linearized as Eq. (5):

$$\frac{t}{q_t} = \frac{1}{k_2\, qe^2} + \frac{t}{q_e} \tag{5}$$

Results obtained from the equation showed that the regression coefficient (R^2) values of Cr (VI) adsorption were closer to 1. That means the most of the adsorption follows the pseudo-second-order kinetic model and it signifies that the chemisorption took place during the reaction. The equilibrium capacities calculated from pseudo-second-order model accepted closely with the capacities found from the isotherm.

Regeneration study

Regeneration and recycling availability of the *n*-fib@Mats are important factors for reusing the adsorbents. By applying this procedure, Cr (VI) can be recovered from the contaminated aqueous phase and lead to reusability of the PAN *n*-fib@Mat, PAN/ZnO *n*-fib@Mat, and PAN/ZnO-TiO_2 *n*-fib@Mat that employed in the adsorption process. This procedure makes the process more useful, cheaper, and related to the removal of Cr (VI). Therefore, four consecutive sorption–desorption cycles were performed by using of 0.1 M HCl to regenerate the PAN *n*-fib@Mat, PAN/ZnO *n*-fib@Mat, and PAN/ZnO-TiO_2 *n*-fib@Mat. The adsorption rate decreased a little bit from 92 to 86% after 4 cycles and the adsorption ability of PAN/ZnO-TiO_2 *n*-fib@Mat decreased 6%. Experimental results showed that the produced PAN/ZnO-TiO_2 *n*-fib@Mat exhibited reasonable adsorption for repeated practical use.

Conclusions

In this study, ZnO-TiO_2 nanoparticles were fabricated by the arc discharge technique. Using these

Table 3 Kinetic parameters of Cr (VI) adsorption onto the nanoparticle decorated PAN based *n*-fib@Mats

	Pseudo-first-order			Pseudo-second-order			
	q_e	$k_1 \times 10^{-2}$	R^2	q_e	$k_2 \times 10^{-3}$	h_o	R^2
	(mg g^{-1})	(min^{-1})		(mg g^{-1})	(g mg^{-1} min^{-1})	(mg g^{-1} min^{-1})	
PAN	212.25	0.12	0.93	158.57	0.208	0.67	0.99
PAN-ZnO	194.71	0.76	0.94	243.91	0.059	3.56	0.98
PAN-ZnO-TiO_2	300.68	2.99	0.97	337.14	0.042	5.33	0.99

nanoparticles, PAN *n*-fib@Mat, PAN-ZnO *n*-fib@Mat, and PAN/ZnO-TiO_2 *n*-fib@Mat were produced by via electrospinning method. PAN *n*-fib@Mat, PAN-ZnO *n*-fib@Mat, and PAN/ZnO-TiO_2 *n*-fib@Mat, which are synthesized, were used as an effective adsorbent for the adsorption of Cr (VI) ions from aqueous solutions. The initial pH solution has a marked influence on the Cr (VI) adsorption performance. The maximum adsorption of Cr (VI) ions was obtained at the equilibrium pH of 2.2. The adsorption equilibrium was reached in 240 min for PAN/ZnO-TiO_2 *n*-fib@Mat and 360 min for PAN *n*-fib@Mat and PAN-ZnO *n*-fib@Mat. The pseudo-second-order model adsorption was selected from the results obtained from the kinetic studies. The SEM results of PAN *n*-fib@Mat exhibits uniform nanofiber-structures with an average diameter of 50 nm to 350 nm. The ZnO-TiO_2 nanoparticles adhered on the surface of *n*-fib@Mat very *clearly in* SEM and TEM images. The isotherm studies revealed that the Langmuir model was well described in the equilibrium for the Cr (VI) and PAN *n*-fib@Mat, PAN/ZnO *n*-fib@Mat, and PAN/ZnO-TiO_2 *n*-fib@Mat interaction. Using the Langmuir isotherm model equation, the maximum adsorption capacities *(Q)* calculated for the interaction of Cr (VI) on the PAN *n*-fib@Mat, PAN/ZnO *n*-fib@Mat, and PAN/ZnO-TiO_2 *n*-fib@Mat were 153.85, 234.52, and 333.43 mg/g, respectively. This study showed that a high amount of Cr (VI) was taken from the aqueous phase by using the PAN *n*-fib@Mat, PAN/ZnO *n*-fib@Mat, and PAN/ZnO-TiO_2 *n*-fib@Mat and PAN/ZnO-TiO_2 *n*-fib@Mat.

Abbreviations

PAN: Polyacrylonitrile; PAN/ZnO *n*-fib@Mat: PAN/ZnO nanofiber-Mat; PAN/ZnO-TiO_2 *n*-fib@Mat: PAN/ZnO-TiO_2 nanofiber-Mat

Acknowledgements

Not applicable.

Authors' contributions

EP and AA conceived of the study and contributed in design and organization of the manuscript. AY produced *n*-fib@Mats. ŞP carried out the adsorption and kinetic experiments. AY and ŞP performed the data analysis. EP and AA did the manuscript writing and execute the data interpretation. All authors read and approved the final manuscript.

Funding

Not applicable.

Availability of data and materials

Research data have been provided in the manuscript.

Competing interests

The authors declare that they have no competing interests.

Author details

[1]Department of Chemical Engineering, Konya Technical University, Campus, 42079 Konya, Turkey. [2]Department of Mechanical Engineering, Bingöl University Campus, 12000 Bingöl, Turkey. [3]Department of Biomedical Engineering, Necmettin Erbakan University, Campus, 42079 Konya, Turkey.

Received: 18 December 2018 Accepted: 30 May 2019
Published online: 20 June 2019

References

Alcaraz-Espinoza JJ, Chavez-Guajardo AE, Medina-Llamas JC, Andrade CA, Melo CP. Hierarchical composite polyaniline-(electrospun polystyrene) fibers applied to heavy metal remediation. ACS Appl Mater Interfaces. 2015;7:7231–40.

Avcı A, Eskizeybek V, Gülce H, Haspulat B, Şahin ÖS. ZnO–TiO2 nanocomposites formed under submerged DC arc discharge: preparation, characterization and photocatalytic properties. App Phy A. 2013;116:1119–25.

Beheshti H, Irani M, Hosseini L, Rahimi A, Aliabadi M. Removal of Cr (VI) from aqueous solutions using chitosan/MWCNT/Fe3O4 composite nanofibers-batch and column studies. Chem Eng J. 2016;284:557–64.

Cao F, McEnaney K, Chen G, Ren ZF. A review of cermet-based spectrally-selective solar absorbers. Energy Env Sci. 2014;7:1615–27.

Esfe MH, Afrand M, Rostamian SH, Toghraie D. Examination of rheological behavior of MWCNTs/ZnO-SAE40 hybrid nano-lubricants under various temperatures and solid volume fractions. Exper Therm Fluid Sci. 2017;80:384–90.

Eskizeybek V, Demir O, Avci A, Chhowalla M. Synthesis and characterization of cadmium hydroxide nanowires by arc discharge method in de-ionized water. J Nanopart Res. 2011;13:4673–80.

Fan LL, Luo CN, Sun M, Qiu HM. Synthesis of graphene oxide decorated with magnetic cyclodextrin for fast chromium removal. J Mater Chem. 2012;22:24577–83.

Gezici O, Guven I, Özcan F, Ertul S, Bayrakci M. Humic-makeup approach for simultaneous functionalization of polyacrylonitrile nanofibers during electrospinning process, and dye adsorption study. Soft Mater. 2016;14(4):278–87.

Hameed BH, Tan IAW, Ahmad AL. Adsorption isotherm, kinetic modeling and mechanism of 2,4,6-trichlorophenol on coconut husk-based activated carbon. Chem Eng J. 2008;144:235–44.

Hanif S, Shahzad A. Removal of chromium (VI) and dye Alizarin Red S (ARS) using polymer-coated iron oxide (Fe 3 O 4) magnetic nanoparticles by co-precipitation method. J Nanopart Res. 2014;16(6):2429.

Kaya K, Pehlivan E, Schmidt C, Bahadir M. Use of modified wheat bran for the removal of chromium (VI) from aqueous solutions. Food Chem. 2014;158:112–7.

Koyuncu H, Kul AR. Removal of aniline from aqueous solution by activated kaolinite: kinetic, equilibrium and thermodynamic studies. Coll Surf A: Phys Eng Asp. 2019;569:59–66.

Langmuir I. The constitution and fundamental properties of solids and liquids. J Frankl Inst. 1917;183:102.

Lee YC, Yang JW. Self-assembled flower-like TiO2 on exfoliated graphite oxide for heavy metal removal. J Ind Eng Chem. 2012;18:1178–85.

Li R, Li Q, Gao S, Shang JK. Exceptional arsenic adsorption performance of hydrous cerium oxide nanoparticles: part a. adsorption capacity and mechanism. Chem Eng J. 2012;127:185–6.

Li W, Yang Z, Meng Q, Shen C, Zhang G. Thermally stable and solvent resistant self-crosslinked TiO2/PAN hybrid hollow fiber membrane fabricated by mutual supporting method. J Memb Sci. 2014;467:253–61.

Liu Q, Liu Q, Liu B, Hu T, Liu W, Yao J. Green synthesis of tannin-hexamethylendiamine based adsorbents for efficient removal of Cr (VI). J Hazar Mater. 2018;352:27–35.

Lv X, Qin X, Wang K, Peng Y, Wang P, Jiang G. Nanoscale zero valent iron supported on MgAl-LDH-decorated reduced graphene oxide: enhanced performance in Cr (VI) removal, mechanism and regeneration. J Hazar Mater. 2019;373(2019):176–86.

Matos MP, Correia AAS, Rasteiro MG. Application of carbon nanotubes to immobilize heavy metals in contaminated soils. J Nanopart Res. 2017;19(4):126.

Mittal J, Bahl OP, Mathur RB, Sandle NK. Ir studies of Pan fibers thermally stabilized at elevated-temperatures. Carbon. 1994;32:1133–6.

Naimi-Joubani M, Shirzad-Siboni M, Yang JK, Gholami M, Farzadkia M. Photocatalytic reduction of hexavalent chromium with illuminated ZnO/TiO_2 composite. J Indus Eng Chem. 2015;22:317–23.

Parlayici Ş. Modified peach stone shell powder for the removal of Cr (VI) from aqueous solution: synthesis, kinetic, thermodynamic, and modeling study. Inter J Phytorem. 2019;21(6):590–9.

Parlayici Ş, Yar A, Avci A, Pehlivan E. Removal of hexavalent chromium using polyacrylonitrile/titanium dioxide nanofiber membrane. Des Water Treat. 2016;57:16177–83.

Parlayici Ş, Pehlivan E. Comparative study of Cr (VI) removal by bio-waste adsorbents: equilibrium, kinetics, and thermodynamic. J Anal Sci Techn. 2019;10(1):15.

Parlayici S, Pehlivan E. Natural biosorbents (garlic stem and horse chesnut shell) for removal of chromium (VI) from aqueous solutions. Env Monitor Assess. 2015;187:763.
Pradhan D, Sukla LB, Mishra BB, Devi N. Biosorption for removal of hexavalent chromium using microalgae Scenedesmus sp. J Clean Pro. 2019;209:617–29.
Qiu B, Gu HB, Yan XR, Guo J, Wang Y, Sun D, Wang Q, Khan M, Zhang X, Weeks BL, Young DP, Guo Z, Wei S. Cellulose derived magnetic mesoporous carbon nanocomposites with enhanced hexavalent chromium removal. J Mater Chem A. 2014;2:17454–62.
Qiu H, Zhang S, Pan B, Zhang W, Lv L. Effect of sulfate on Cu (II) sorption to polymer-supported nano-iron oxides: behavior and XPS study. J Coll Inter Sci. 2012;366(1):37–43.
Solomon MFJ, Bhole Y, Livingston AG. High-flux hydrophobic membranes for organic solvent nanofiltration (OSN)-interfacial polymerization, surface modification and solvent activation. J Memb Sci. 2013;434:193–203.
Su Q, Pan B, Pan B, Zhang Q, Zhang W, Lv L, Wang X, Wu J, Zhang Q. Fabrication of polymer-supported nanosized hydrous manganese dioxide (HMO) for enhanced lead removal from waters. Sci Total Env. 2009;407:5471–7.
Toghraie D, Chaharsoghi VA, Afrand M. Measurement of thermal conductivity of ZnO–TiO 2/EG hybrid nanofluid. J Therm Analy Calor. 2016;125(1):527–35.
Wang JQ, Pan K, Giannelis EP, Cao B. Polyacrylonitrile/polyaniline core/shell nanofiber mat for removal of hexavalent chromium from aqueous solution: mechanism and applications. RSC Adv. 2013;3:8978–87.
Yang ZH, Zhang GL, Liu FN, Meng Q. Physicochemical characteristics of hollow fiber structured packings in isopropanol/water distillation. Ind Eng Chem Res. 2010;49:11594–601.
Yuan P, Liu D, Fan MD, Yuana P, Liua D, Fana M, Yanga D, Zhuc R, Gec F, Zhua JX, He H. Removal of hexavalent chromium [Cr (VI)] from aqueous solutions by the diatomite-supported/unsupported magnetite nanoparticles. J Hazard Mater. 2010;173:614–21.

Publisher's Note